Thermo-optic microring resonator switching elements made of dielectric-loaded plasmonic waveguides

Odysseas Tsilipakos,[1,a)] Emmanouil E. Kriezis,[1,b)] and Sergey I. Bozhevolnyi[2]
[1]*Department of Electrical and Computer Engineering, Aristotle University of Thessaloniki, Thessaloniki GR-54124, Greece*
[2]*Institute of Sensors, Signals, and Electrotechnics (SENSE), University of Southern Denmark, Niels Bohrs Allé 1, DK-5230 Odense M, Denmark*

(Received 6 December 2010; accepted 17 February 2011; published online 11 April 2011)

Thermo-optic switching elements made of dielectric-loaded plasmonic (DLSPP) waveguides are theoretically investigated by utilizing the three-dimensional vector finite element method. The configurations considered employ microring resonators, whose resonant frequency is varied by means of thermal tuning. First, a classic add-drop filter with parallel access waveguides is examined. Such a component features very poor drop port extinction ratio (ER). We therefore extend the analysis to add-drop filters with perpendicular access waveguides, which are found to exhibit superior drop port ERs, due to interference effects associated with the drop port transmission. In the process, the performance of a DLSPP waveguide crossing is also assessed, since it is a building block of those filters whose bus waveguides intersect. An elliptic tapering scheme is proposed for minimizing cross talk and its effect on the filter performance is explored. The dual-resonator add-drop filter with perpendicular bus waveguides and an untreated waveguide crossing of Sec. V A can act as an efficient 2×2 switching element (the single-resonator variant can only act as a 1×2 switch due to structure asymmetry), possessing two equivalent input ports and featuring high ERs for both output ports over a broad wavelength range. Specifically, an extinction ratio of at least 8 dB can be attained for both output ports over a wavelength range of 3.2 nm, accommodating four 100-GHz-spaced channels. Switching times are in the order of a few microseconds, rendering the aforementioned structure capable of handling real-world routing scenarios. © *2011 American Institute of Physics*. [doi:10.1063/1.3564949]

I. INTRODUCTION

Guided-wave plasmonics, a research area concerned with the manipulation and routing of guided plasmonic modes, has attracted considerable attention in recent years. Plasmonic waveguides comprising at least one metal-dielectric interface can support modes having spot sizes of subwavelength dimensions. As a result, plasmonic components can be used to build nanophotonic integrated circuits, combining the bandwidth of photonics along with nanoscale dimensions.[1–3] However, in order to assemble fully operational plasmonic circuits, one must first address the need for efficient switching/routing elements.

To date, several 2D plasmonic waveguides, i.e., able to confine light in both transverse directions, have been demonstrated. The recently proposed dielectric-loaded plasmonic (DLSPP) waveguide[4] offers some distinct advantages compared to other alternatives. It is technologically simple, consisting of a dielectric or polymer ridge deposited on a metallic film, and exhibits strong guiding properties along with relatively small propagation losses ($L_{prop} \sim 50$ μm for the fundamental TM_{00} mode). More importantly, the DLSPP waveguide is the only plasmonic waveguide with tight mode confinement that has been employed in the realization of thermo-optic components. The stripe plasmonic waveguide[5,6] has also been utilized for this task,[7,8] but the long-range mode it supports lacks strong confinement having a spot size which spans several microns in both lateral directions.[9]

Among the DLSPP-based components that have been demonstrated, wavelength-selective ones[10–12] are of substantial interest. By providing such components with tuning capabilities, e.g., through the thermo-optic effect, they can be transformed from mere filters into switching elements, thus making fully functional plasmonic circuits possible. As mentioned earlier, DLSPP-based thermo-optic components have already been proposed, including microring resonator filters and Mach-Zehnder interferometers. Their switching capabilities have been theoretically analyzed and experimentally proven.[13,14] It is worth noting that thermo-optic control is naturally compatible with DLSPP-based components, since the same thin metal circuitry used for supporting the plasmonic mode can be used for carrying the control current as well. Thus, there is no need for extra heating circuits. More importantly, such components can be quite efficient, since the supported mode exhibits its maximum just above the metal-dielectric interface. Obviously, the temperature increase due to ohmic heating induced by the control current is at its maximum near that same interface too, resulting in relatively small power consumption requirements for the aforementioned components. Finally, a proper choice of the substrate on which the DLSPP-based component is residing can provide switching times of a few microseconds, rendering the thermally-tunable component suitable for practical

a)Electronic mail: otsilipa@auth.gr.
b)Electronic mail: mkriezis@auth.gr.

 © 2011 American Institute of Physics

Downloaded 18 Apr 2011 to 155.207.26.21. Redistribution subject to AIP license or copyright; see http://jap.aip.org/about/rights_and_permissions

applications. In fact, both heat-up and cool-down time constants of the thermal response are approximately equal to 1.35 μs,[13] since, as revealed by transient thermal modeling simulations, the lower part of the polymer ridge, which accommodates most of the TM_{00} mode, is the first to heat-up as well as cool-down.

The main factor limiting the performance, and thus the practical perspective, of such switching elements is the rather small thermo-optic coefficient (TOC) of the polymers used currently as loadings. In the case of resonator-based components, this means that the maximum thermo-optic shift (limited by the maximum temperature sustained by the polymer) is less than half the free spectral range (FSR).[13] As a result, the actually attainable extinction ratio (ER) is smaller than the maximum available, which is simply the maximum to minimum transmission contrast. The obvious way of improving the performance of such components is by supplying polymers with higher TOCs. However, even more important is to identify the switching configuration leading to optimum performance given the currently available loading materials.

In this work, we address the need for efficient DLSPP-based switching elements by comparing the performance of several thermo-optic components employing microring resonators. We adopt the standard thermo-optic coefficient of -1.05×10^{-4} K^{-1}, corresponding to poly-methyl-methacrylate (PMMA), and attempt to determine the optimum, in terms of ER, switching configuration. PMMA is chosen as the loading material since it has been widely used in the realization of dielectric-loaded plasmonic waveguides and components.[10,11,14–17] Regarding the geometrical and material properties adopted for the DLSPP waveguide: The dimensions of the PMMA ridge are $w \times h = 500 \times 600$ nm^2, ensuring single-mode operation in the wavelength range of interest (1.52 – 1.57 μm),[4] and the refractive index at room temperature is 1.493. Furthermore, the metallic stripe on which the polymer is residing is made of gold whose refractive index is taken from Ref. 18 and equals $0.55 - j11.5$. The gold stripe is 100 nm thick and 3 μm wide. It is for the purpose of thermal addressing that the metallic film is restricted into having a finite width (3 μm). Width values smaller than 3 μm result in a gradual decrease of the propagation length with respect to the reference case of infinite width,[19] and are, thus, avoided. Finally, the combined structure of polymer ridge and gold stripe resides on top of a 1 μm-thick silica layer followed by a silicon substrate, i.e., a typical silicon-on-insulator (SOI) substrate. The numerical investigation of every component considered in this work is conducted by means of three-dimensional vectorial finite element method (3D-FEM) simulations. Details of the method implementation can be found in Ref. 20.

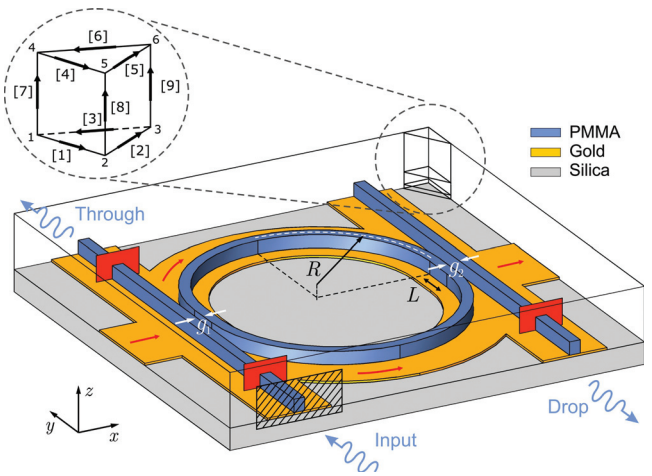

FIG. 1. (Color online) Schematic of a DLSPP-based racetrack resonator add-drop filter with parallel access waveguides and bounding box of the 3D computational domain. The orientation of the triangular prism mesh as well as the element itself with node and edge numbering are also included. For illustration clarity only one prism per material layer is drawn—more are actually used. The input port at which the mode is fed is marked by a ruled rectangle. Fictitious power ports at which guided power is calculated for the input, through, and drop ports are also depicted. Arrows indicate the route of the control current in the event of heating.

The paper is organized as follows: In Sec. II we assess the performance of classic add-drop filters with parallel access waveguides. The main drawback of this component is found to be the poor drop port ER and thus alternative designs are sought for in Secs. IV and V. Before doing so, Sec. III deals with DLSPP-waveguide crossings, since they are encountered in the filters of the sections to come. An elliptic tapering scheme is proposed for minimizing cross talk. Subsequently, add-drop filters with perpendicular access waveguides are considered. This is the objective of Sec. IV. Both treated and untreated waveguide crossings are employed and their effect on the filter performance is explored. The drop port ER is greatly improved with respect to classic add-drop filters, but due to the asymmetry of the structure only one input port can be exploited resulting in a 1×2 switching element. The next section, Sec. V, addresses this issue by introducing a second resonator. Again, the utilization of treated or untreated crossings is discussed. Finally, in Sec. VI we provide the summary and the concluding remarks.

II. CLASSIC ADD-DROP FILTER

Add-drop filters consist of a resonator coupled to two parallel access waveguides (Fig. 1). The output waveguide provides an outlet for the rejected wavelengths satisfying the resonance condition. In a simplified approach, we can describe the coupling between resonator and each waveguide by a scattering matrix of the form[13,21]

$$e^{j\theta_0^{(i)}} \begin{bmatrix} t_i & j\sqrt{1-|t_i|^2} \\ j\sqrt{1-|t_i|^2} & t_i^* \end{bmatrix}, \tag{1}$$

where t_i is a complex coefficient, i.e., $t_i = |t_i|\exp(\theta_t^{(i)})$, and we have assumed that the coupling is lossless. Assuming additionally that a single unidirectional mode is excited in the resonator, and that no reflections are present, one can end up with the following expressions for the port transmission

$$T_{\text{thru}} = \frac{\alpha^2|t_2|^2 + |t_1|^2 - 2\alpha|t_1||t_2|\cos(\theta - \theta_{\text{CIFS}})}{1 + \alpha^2|t_1|^2|t_2|^2 - 2\alpha|t_1||t_2|\cos(\theta - \theta_{CIFS})}. \tag{2a}$$

$$T_{\text{drop}} = \frac{(1-|t_1|^2)(1-|t_2|^2)\alpha}{1 + \alpha^2|t_1|^2|t_2|^2 - 2\alpha|t_1||t_2|\cos(\theta - \theta_{\text{CIFS}})}, \tag{2b}$$

Downloaded 18 Apr 2011 to 155.207.26.21. Redistribution subject to AIP license or copyright; see http://jap.aip.org/about/rights_and_permissions

In the above equations, θ is the phase accumulated by the mode per circulation given by $(2\pi/\lambda)\mathrm{Re}[n_{\mathrm{eff}}(\lambda)](2\pi R+2L)$, and α stands for the loss in the resonator, comprising both resistive and bend losses. Consequently, after one round trip, the field amplitude of the circulating mode is scaled by the complex factor $\alpha\exp(-j\theta)$. θ_{CIFS} accounts for the shift in the resonant frequency of the coupled, with respect to the uncoupled, resonator, i.e., the coupling-induced frequency shift (CIFS),[21] and equals $\theta_0^{(1)}+\theta_0^{(2)}-\theta_t^{(1)}-\theta_t^{(2)}$. In what follows, Eqs. 2 will be used to qualitatively complement the rigorous 3D-FEM simulations.

A schematic of the simulated structure along with the main geometrical parameters is depicted in Fig. 1. The (edge-to-edge) gaps separating the resonator from input and output waveguides are designated as g_1 and g_2, respectively. Note also that the resonator radius R is referring to the fictitious circumference located midway between the inner and outer ring boundaries. In general, the resonator is a racetrack ($L\neq 0$). This can become useful if there are fabrication limits on the minimum achievable gap values. In this case, the straight segment of the racetrack resonator can help in increasing the interaction length between resonator and input waveguide, so as to reach the necessary coupling strength leading to critical coupling. As mentioned in Sec. I and evident form Fig. 1, the gold film is patterned, in order to restrict the control current injected for heating purposes. The gold stripe width is 3 μm. Although such a value is adequate for a straight DLSPP waveguide, a larger value might have been advantageous for the resonator, where the waveguide is bent and the circulating mode shifted toward the outward radial direction. However, retaining a small width value is crucial to the power consumption of the component. In order to satisfy both demands, we suggest that the polymer ridge be asymmetrically placed on the metallic ring (Fig. 1). Specifically, with respect to the center of the bent waveguide, the metallic ring extends 1 μm toward the inward and 2 μm toward the outward direction.

Let us now investigate the performance of such components. For this purpose, we calculate the transmission of the through and drop ports for both unheated and heated ($\Delta T=100$ K) states. In order to determine the temperature and thus polymer refractive index distribution in the heated state, we conduct thermal modeling simulations. Steady-state analysis reveals that upon heating the waveguide cross-section (gold stripe and polymer ridge) acquires a constant (spatially-independent) temperature. Moreover, as is evident from Fig. 1, the only polymer parts that will not become heated are the extreme portions of the access waveguides. The rest of the polymer circuit, including resonator and both coupling regions, is going to be uniformly heated by the control current. Thus, it is sound to adopt the same refractive index for the entire polymer circuit. Given the TOC of PMMA, we model the heated state by appointing a reduced by 0.0105 refractive index value, i.e., 1.4825 instead of 1.493, to all polymer regions. For thermal modeling simulation details including the equations solved and material parameters adopted the interested reader can resort to Ref. 13.

We are going to limit the discussion to the wavelength range $1.52-1.57$ μm, spanning the entire C-band. Since the FSR is in the order of 50 nm for the resonator circumferences considered, only one through port transmission dip will be visible. Obviously, more transmission dips would appear if shorter or longer wavelengths were included. We consider an add-drop filter with the following geometrical parameters: $R=5.5$ μm, $L=0.5$ μm, $g_1=0.3$ μm, and $g_2=0.6$ μm. Regarding these choices, the 5.5 μm radius value is a favorable compromise between competing resistive and radiation losses. It leads to minimum overall losses, and consequently maximum quality factors, for the resonator resonances. This has been verified by eigenvalue simulations of the uncoupled resonator. Alternatively, it can be confirmed by transmission simulations of circular 90-degree waveguide bends, like the ones performed in Ref. 22 for slightly different waveguide parameters. The g_1 gap is set to 0.3 μm since smaller values can be challenging from a fabrication standpoint. Then, a straight racetrack segment of 0.5 μm is employed, in order to sufficiently approach critical coupling. The value appointed to g_2 will be justified by the considerations of the following paragraphs.

Figure 2 depicts the transmission curves for both output ports and both states of the aforementioned filter. Clearly, heating shifts the transmission curves toward shorter wavelengths due to the negative TOC of PMMA. By comparing the transmission between different states one can specify the extinction ratio for each port. For example, if we fix the operating wavelength at the maximum of the drop port transmission in the unheated state (1.543 μm), we find an extinction ratio of 11.5 and 2.5 dB for the through and drop port, respectively (Fig. 2). Obviously, the drop port ER is very poor. It can reach a maximum value of 3.5 dB for a different choice of the operating wavelength (1.53 μm), but not higher. Clearly, high ERs (>5 dB) are essential for a tunable component intended as a switching element. Another characteristic of the drop port transmission is the large insertion loss (IL) it experiences; a consequence of the large g_2 gap. However, we assume that ILs in the order of -10 dB are acceptable.

We can easily obtain even higher values for the through port ER by properly adjusting the coupling efficiency between input waveguide and resonator, e.g., by adopting larger L values, so as to further approach critical coupling. This is quite similar to the case of all-pass filters. After all, the presence of the output waveguide, as far as the through port is concerned, is just another loss mechanism, adding to resistive and radiation losses. Specifically, the critical coupling condition $|t_1|=\alpha$ that holds for all-pass filters is simply modified to $|t_1|=\alpha|t_2|$ for add-drop filters [Eq. 2(a)], factoring in the new loss mechanism of light coupling to the output waveguide.

However, the case is very different for the drop port. It is the ER of this port that is the bottleneck of the filter performance and unfortunately it cannot be substantially improved. This is because of the fact that the drop port is not a result of interference and therefore the coupling strength cannot be used as a means of improving the ER, as in the case of the through port. The only way of boosting the drop port ER is by increasing the second gap so as to zero out the drop port transmission minima. The transmission maxima drop accordingly but the ratio is slightly improved. This

Downloaded 18 Apr 2011 to 155.207.26.21. Redistribution subject to AIP license or copyright; see http://jap.aip.org/about/rights_and_permissions

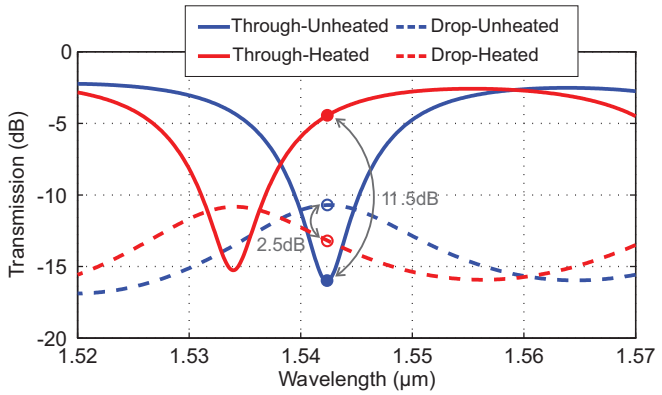

FIG. 2. (Color online) Transmission vs wavelength for both output ports and both heated and unheated states. The geometrical parameters of the add-drop filter with parallel access waveguides are: $R = 5.5\ \mu$m, $L = 0.5\ \mu$m, $g_1 = 0.3\ \mu$m, and $g_2 = 0.6\ \mu$m.

behavior is consistent with the one predicted by Eq. 2(b), according to which the maximum to minimum drop port transmission contrast in dB, i.e., the ER in the ideal scenario where the TOC would suffice for a shift equal to FSR/2, is given by

$$ER_{\text{drop}}^{\text{ideal}} = 10\log_{10}\left(\frac{(1+\alpha|t_1||t_2|)^2}{(1-\alpha|t_1||t_2|)^2}\right). \tag{3}$$

Increasing g_2 results in an increase of the respective t coefficient, and therefore higher drop port ERs. One can now understand why g_2 was initially set to a rather large value. Unfortunately, the improvement is not significant. Moreover, the increase of g_2 leads to even higher insertion losses for the drop port. It is the round trip loss that limits the maximum attainable ER and while it affects the through port as well, it is more detrimental to the drop port ER, due to the absence of interference phenomena, which can be advantageously exploited.

To recapitulate, the DLSPP-based add-drop filter with parallel access waveguides suffers from poor drop port ER. Even if a large g_2 value is adopted (the only way of boosting the drop port ER) the performance of the 1×2 switch remains inadequate for practical applications. What is more,

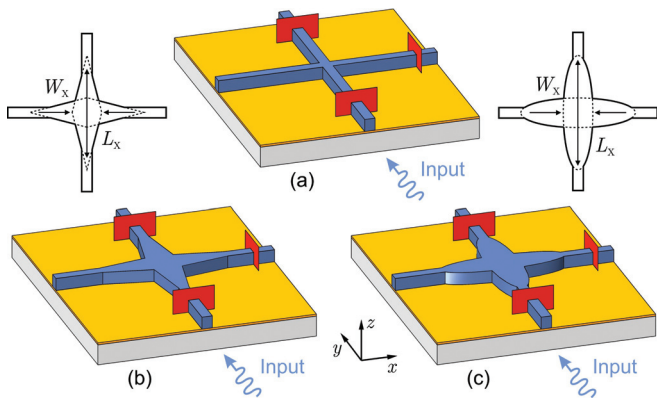

FIG. 3. (Color online) Schematic of an (a) untreated, (b) treated by means of linear tapering, and (c) treated by means of elliptical tapering DLSPP waveguide crossing. The dimensions of the rhombi and ellipses used for constructing the treated crossings are noted in the insets. Fictitious power ports at which guided power is calculated are also depicted.

if we were to equate g_2 with g_1, in order to obtain a 2×2 switching element, the drop port ER would be even worse. In Sec. IV we address this problem by investigating an alternative configuration, namely the add-drop filter with perpendicular access waveguides. This variant may exhibit superior performance due to two reasons. Firstly, light coupling to the perpendicular waveguide in the region of the waveguide intersection renders the drop port transmission a result of interfering waves, thus providing a valuable degree of freedom in shaping the drop port transmission. Secondly, the input-drop route in this case involves only a quarter instead of half the circumference. Before exploring the response of such filters, we examine the waveguide crossing on its own.

III. WAVEGUIDE CROSSING

In this section, we investigate the performance of a DLSPP waveguide crossing, i.e., two intersecting DLSPP waveguides perpendicular to each other [Fig. 3(a)]. For this purpose, we feed one of the waveguides and calculate the normalized guided power (transmission) past the crossing in both waveguides. The performance can be quantified by the IL, i.e., transmission in input waveguide past the crossing, and the XT, i.e., transmission in perpendicular waveguide past the crossing. Obviously, the insertion loss is due to scattering and reflection from the crossing, as well as coupling to the perpendicular waveguide (cross talk). In calculating the IL and XT values, propagation (resistive) losses do not enter in the result, since we treat the crossing as a lumped component. Specifically, we calculate the guided power at some distance from the crossing [Fig. 3(a)] and subsequently correct the computed value with a proper scaling factor compensating for the propagation losses.

The simulated structure is depicted in Fig. 3(a). For an operating wavelength of 1.55 μm, the insertion loss is -0.5 dB and the cross talk -15 dB, respectively. By observing the dominant electric field component (E_z) distribution [Fig. 4(a)], one can verify that some light does indeed couple to the perpendicular waveguide while some is lost via scattering. Similar values for the insertion loss and cross talk have been reported in silicon photonics as well.[23] The performance there is a little worse (IL ~ -1 dB and XT ~ -9 dB) due to the slightly tighter mode confinement. This can be explained by the following reasoning: During the extent of the crossing the mode tends to spread out laterally due to the momentary absence of waveguide walls. The tighter the field confinement in the waveguide, the stronger the diffraction effects in the intersection, making the spreading more pronounced. Clearly, wider spreading results in easier coupling to the perpendicular waveguide, i.e., higher cross talk, leading to higher insertion losses as well. In short, it is the level of mode confinement that dictates the performance of a waveguide crossing. This has been demonstrated with metal-insulator-metal (MIM) plasmonic waveguides.[24] The deep sub-wavelength confinement possible with such waveguides gives rise to interesting results in MIM waveguide junctions.

In many occasions, cross talk is undesirable. Although the XT of the untreated waveguide crossing (-15 dB) may seem rather low, it is actually not negligible. Specifically, if

Downloaded 18 Apr 2011 to 155.207.26.21. Redistribution subject to AIP license or copyright; see http://jap.aip.org/about/rights_and_permissions

an input wave of unit amplitude impinges on the crossing, the wave traveling in the perpendicular waveguide (either direction) has an amplitude of approximately 0.2. As discussed earlier, the level of cross talk is proportional to the level of mode confinement. Thus, the cross talk can be suppressed by relaxing the mode confinement just before it arrives at the waveguide intersection. This can be done by treating the waveguide crossing, i.e., providing some kind of tapering which would be responsible for expanding the guided mode. Both linear [Fig. 3(b)] and elliptical [Fig. 3(c)] tapering shapes were considered having several values of tapering widths (W_X) and lengths (L_X). The linear tapering scheme consists of two identical rhombi perpendicular to each other, centered at the waveguide intersection. The short diagonal is equal to W_X and the large diagonal equal to L_X [inset of Fig. 3(b)]. In the same way, the elliptical tapering scheme consists of two identical ellipses centered at the waveguide intersection. This time, the minor axis is equal to W_X and the large axis equal to L_X [inset of Fig. 3(c)].

Next, a parametric study is performed in order to determine the optimum tapering dimensions for minimizing cross talk. We found that the tapering length of 6 μm is a favorable compromise between smooth mode expansion and compactness. We therefore fix L_X to 6 μm and vary the tapering width W_X. In general, as W_X increases cross talk is suppressed for both tapering shapes. However, elliptical tapering was found to provide the best balance between low XT and small ILs. Specifically, for such a tapering shape, cross talk reaches a minimum for a width value of 1.6 μm [Fig. 5(a)]. Larger values of W_X along with linear tapering can provide comparable levels of cross talk, but they are accompanied by increased ILs as the unconfined region length increases. They are therefore discarded.

Given the above, for the purpose of minimizing cross talk, we conclude to an elliptic tapering shape with $L_X = 6$ μm and $W_X = 1.6$ μm. For an operating wavelength of 1.55 μm these dimensions result in a cross talk of ~ -37 dB and an insertion loss of ~ -0.8 dB, only slightly larger than that of the untreated crossing (0.5 dB). The distribution of the dominant electric field component in this case is depicted in Fig. 4(b). As can be seen, cross talk is greatly suppressed.

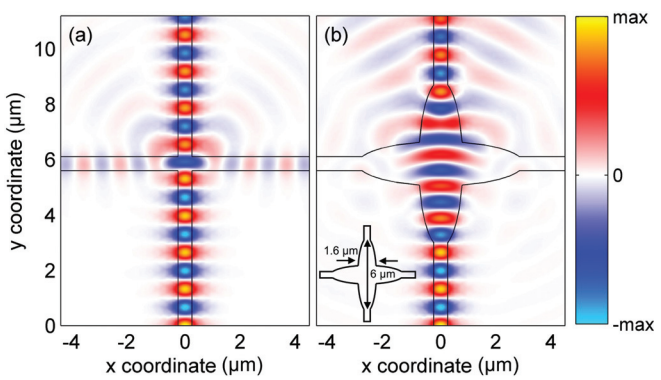

FIG. 4. (Color online) Distribution of the dominant electric field component (E_z) in an (a) untreated and (b) treated by means of elliptical tapering ($L_X = 6$ μm, $W_X = 1.6$ μm) DLSPP waveguide crossing. The real part of the E_z component is plotted at an xy-plane located 10 nm above the metal surface.

On the other hand, scattering losses have increased. Figure 5(b) depicts the wavelength dependence of the treated crossing performance (IL and XT) for this optimum case. Evidently, the wavelength dependence is very weak. Specifically, the cross talk remains smaller than -35 dB in the entire C-band, while the IL is almost constant, exhibiting a variation of approximately 0.02 dB.

IV. ADD-DROP FILTER WITH PERPENDICULAR ACCESS WAVEGUIDES

Having determined the performance of DLSPP waveguide crossings, we now turn to add-drop filters with perpendicular access waveguides (also termed cross-connect filters). Such components are widely used in other photonics technologies as building blocks of complex filtering/routing configurations.[25–27] Schematics of such filters, having both untreated and treated waveguide crossings, are depicted in Fig. 6.

The treated-crossing variant [Fig. 6(b)] is very similar to the classic add-drop filter with parallel access waveguides of Sec. II. Some minor differences are the following: Firstly, the insertion loss for the through port is anticipated to be slightly higher, due to the presence of the crossing introducing extra losses (~ 0.8 dB according to Sec. III) and resulting in a slightly longer input-through port separation. Secondly, the input-drop route involves only a quarter instead of half the resonator circumference. However, this does not lead to superior ER for the drop port, as one might expect. It merely corresponds to lower insertion losses. This can be verified by writing down a transmission equation like the one derived for the drop port of the classic add-drop filter. It turns out that this equation is identical to Eq. 2(b), except from the fact that α in the nominator is substituted by $\sqrt{\alpha}$. Clearly, this does not affect the ideal drop port extinction ratio which is given again by Eq. 3. It only means that the insertion losses for both states will be somewhat smaller, since $\alpha < 1$. As a result, the add-drop filter with perpendicular access waveguides and a treated crossing cannot tackle the problem of poor drop port ER.

More interesting is the untreated-crossing variant [Fig. 6(a)]. In this case, the drop port transmission becomes a result of interfering waves: the one via the ring and the one coming from the crossing. This means that by properly tuning the geometrical parameters we can get very small drop port transmission minima (due to destructive interference) and therefore achieve high ERs for the drop port. For this purpose, the g_2 gap must be relatively large so that the two interfering waves are of comparable amplitude. If g_2 is too small the amplitude of the wave via the ring is substantially higher and the two waves cannot cancel each other out. Obviously, this means that there is no need for a straight segment in this interaction region.

Let us examine an add-drop filter of this type with the following geometrical parameters: $R = 5.5$ μm, $L = 0.5$ μm, $g_1 = 0.3$ μm, and $g_2 = 0.6$ μm. They are identical to those of the classic add-drop filter studied in Sec. II. All parameter values are carefully selected so as to ensure high performance in terms of ER. The reasons behind each choice have

Downloaded 18 Apr 2011 to 155.207.26.21. Redistribution subject to AIP license or copyright; see http://jap.aip.org/about/rights_and_permissions

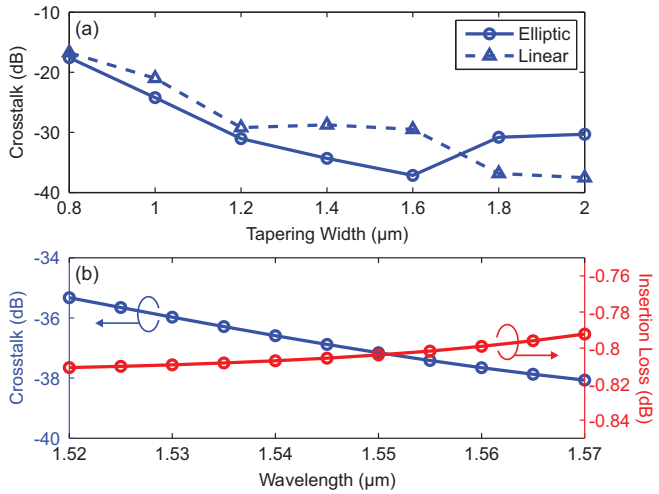

FIG. 5. (Color online) (a) Cross talk vs tapering width for linear (triangular markers) and elliptical (circular markers) tapering shapes. (b) Cross talk and insertion loss as functions of the operating wavelength for the optimum configuration: elliptic tapering with $W_X = 1.6$ μm. L_X is constant and equal to 6 μm throughout.

been already highlighted. The transmission curves for the aforementioned filter (both ports and both states) are depicted in Fig. 7. In addition, the drop port transmission for the case of treated crossing (unheated state) is also included (dotted curve) for comparison purposes. Clearly, interference effects have reshaped the drop port transmission curve introducing steeper segments which can lead to improved ERs. Specifically, by fixing the operating wavelength at 1.531 μm we measure an ER of approximately 9 dB for both ports (Fig. 7). Note also that the maximum of the drop port transmission no longer coincides with the minimum of the through port transmission; again due to the same interference effects.

The effect of cross talk on the shape of the drop port transmission curve has been also noted in the context of silicon photonics.[27,28] However, due to the different conditions (mainly the absence of significant propagation losses), cross talk does not seem to enhance the optical response and, thus, tapering schemes are employed to suppress it.[26,27]

To summarize, we can realize efficient 1×2 switching elements featuring high ERs for both output ports by employing add-drop filters with perpendicular, instead of parallel, access waveguides. The waveguide crossing must be left untreated, so that the drop port transmission becomes a result of interfering waves. However, such structures do not have two equivalent input ports and cannot act as 2×2 switches. First, because in order to obtain high ERs for the drop port a large value must be appointed to g_2. This means that the coupling conditions between the resonator and the two access waveguides are different. Moreover, even if we were to impose identical coupling conditions, i.e., $g_2 = g_1$ and $L = 0$, and were willing to accept the relatively poor performance which accompanies them, the symmetry would still be broken. For example, one can easily confirm that the input-drop route for the first input involves one quarter, while the one for the second input three quarters of the resonator circumference. This issue is addressed in the following section by introducing a second microring resonator.

V. DUAL-RESONATOR ADD-DROP FILTER WITH PERPENDICULAR ACCESS WAVEGUIDES

Schematics of dual-resonator add-drop filters with perpendicular access waveguides, having both untreated and treated waveguide crossings, are depicted in Fig. 8. Again, the gold film is patterned so as to restrict the control current in the event of heating. We should note that sharp corners in the metallic film patterning should be avoided, since they can result in high current density values and accordingly high local temperatures damaging the polymer. As a result, in an actual implementation, any sharp corners, like those about the waveguide crossing, should be chamfered. Regarding filter operation, the addition of the second ring renders the structure symmetric, meaning that one can now find two equivalent input ports even when the coupling conditions

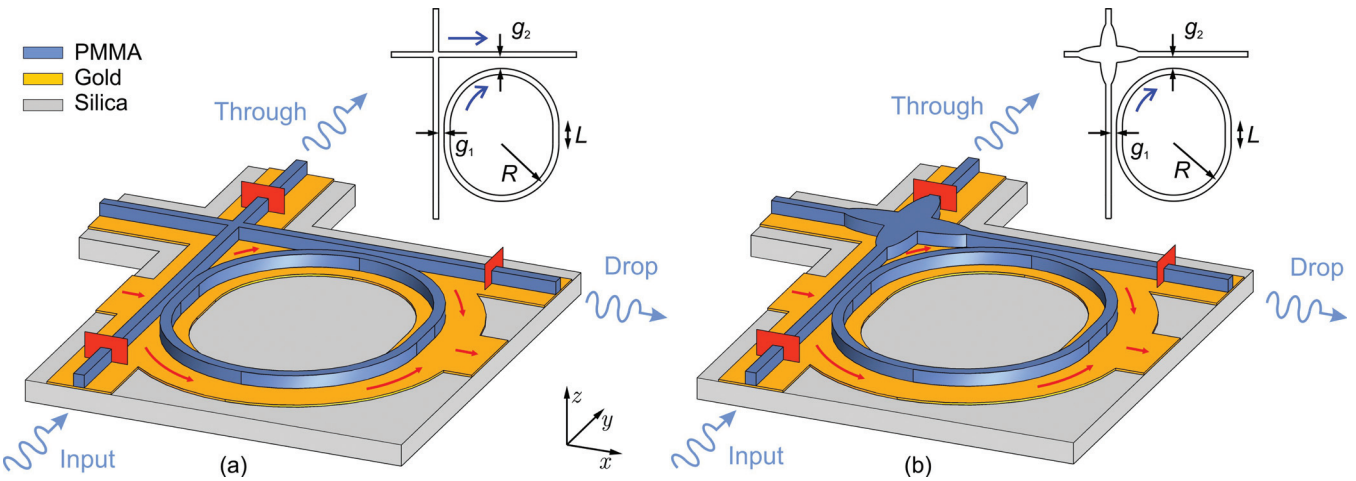

FIG. 6. (Color online) Schematic of a DLSPP-based add-drop filter with perpendicular access waveguides and an (a) untreated or (b) treated by means of elliptical tapering ($L_X = 6$ μm, $W_X = 1.6$ μm) waveguide crossing. Fictitious power ports at which guided power is calculated for the input, through, and drop ports are also shown. Arrows indicate the route of the control current in the event of heating. The insets depict the main geometrical parameters and the interfering waves shaping the drop port transmission.

Downloaded 18 Apr 2011 to 155.207.26.21. Redistribution subject to AIP license or copyright; see http://jap.aip.org/about/rights_and_permissions

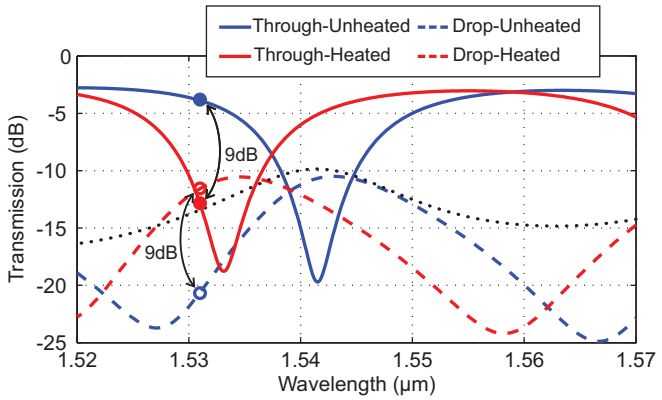

FIG. 7. (Color online) Transmission vs wavelength for both output ports and both heated and unheated states. The geometrical parameters of the single-resonator add-drop filter with perpendicular access waveguides and an untreated crossing are: $R = 5.5$ μm, $L = 0.5$ μm, $g_1 = 0.3$ μm, and $g_2 = 0.6$ μm. The drop port transmission for an identical filter but with a treated crossing (unheated state) is also depicted with a dotted curve.

between resonator and input or output waveguide are different (i.e., $g_1 \neq g_2$ or $L \neq 0$). Thus, the structure can act as a 2×2 switching element. Needless to say that for this to hold the input waveguide-resonator and output waveguide-resonator coupling conditions should be identical for both resonators [see insets of Fig. 8]. Except from restoring the symmetry, the presence of the second resonator introduces an extra route to the drop port. We name this path "Q-route" due to the shape of its trace [see insets of Fig. 8]. This means that even if the crossing is treated, the drop port transmission is still a result of interfering waves. Compared to the single-resonator filters of the previous sections, the through port ILs are anticipated to increase, due to the longer input-through port separation. Finally, the linewidth of the through port transmission minimum is bound to be broader since the wave traveling toward the through port encounters two resonators whose through port transmission functions are almost centered (almost due to the different CIFS when $g_1 \neq g_2$ $L \neq 0$).

A. Untreated waveguide crossing

Let us first focus on the untreated-crossing variant [Fig. 8(a)]. The drop port transmission in this case is the result of three interfering waves: the one via the resonator, the one coming from the crossing, and the one following the Q-route [inset of Fig. 8(a)]. We have already stressed that it is exactly these interference effects that can be advantageously exploited leading to high ERs for the drop port.

As an example, we examine a filter of this type with the following geometrical parameters: $R = 5.5$ μm, $L = 0$, $g_1 = 0.3$ μm, and $g_2 = 0.5$ μm. This time, we do not employ a racetrack resonator since it is not the through port ER that limits the filter performance. Again, the g_2 gap is rather large. If g_2 is too small the amplitude of the wave via the ring is substantially higher than the other two, meaning that no cancellation of the interfering waves is to be expected.

The transmission for both ports and states is depicted in Fig. 9(a). Again, the irregular shape of the drop port transmission curve demonstrates the presence of interference effects. Due to this complex curve shape, the operating wavelengths leading to high ERs simultaneously for both ports are hard to identify. To this end, we plot in Fig. 9(b) the ER for both ports in the entire wavelength range. We are interested in continuous wavelength regions that can provide high extinction ratios for both ports simultaneously. As can be seen, an ER better than 5 dB can be provided by two wavelength regions with an aggregate size of 10 nm. This wavelength span can accommodate twelve WDM (wavelength-division multiplexing) channels with 100 GHz (0.8 nm) spacing. Alternatively, if we define the ER threshold at 8 dB we find a single wavelength region of 3.2 nm (four 100-GHz spaced WDM channels) that can provide it. The optimum

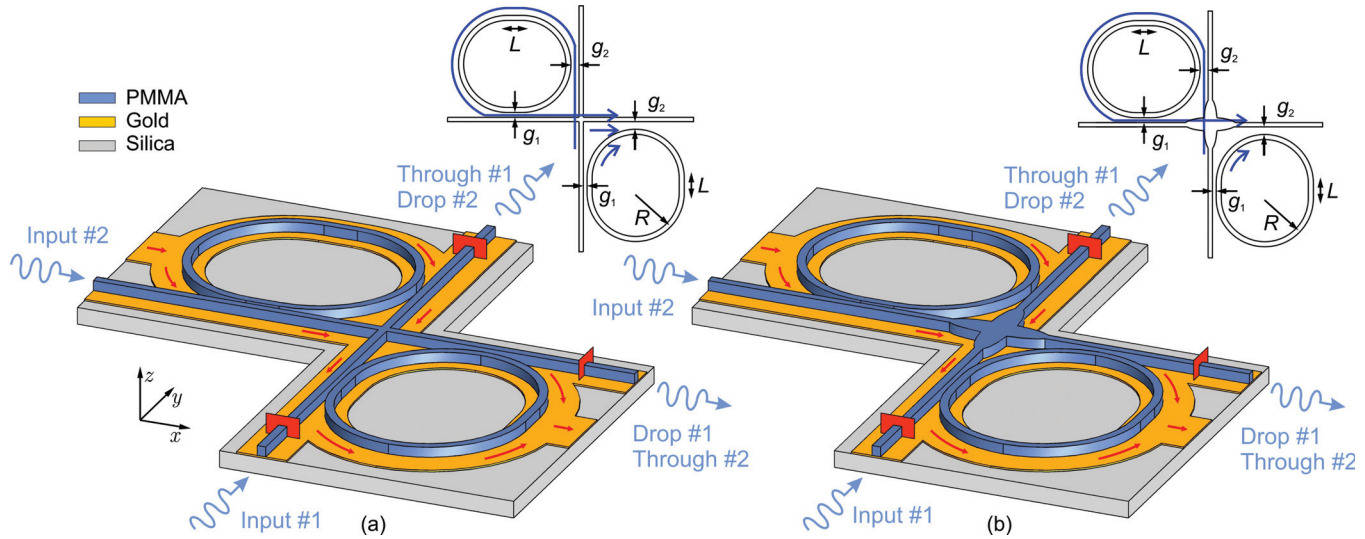

FIG. 8. (Color online) Schematic of a DLSPP-based dual-resonator add-drop filter with perpendicular access waveguides and an (a) untreated or (b) treated by means of elliptical tapering ($L_X = 6$ μm, $W_X = 1.6$ μm) waveguide crossing. Fictitious power ports at which guided power is calculated for the input, through, and drop ports are also shown. Arrows indicate the route of the control current in the event of heating. The insets depict the main geometrical parameters and the interfering waves shaping the drop port transmission.

Downloaded 18 Apr 2011 to 155.207.26.21. Redistribution subject to AIP license or copyright; see http://jap.aip.org/about/rights_and_permissions

performance is achieved at the operating wavelength of 1.537 μm, where the ERs are 10.8 and 9 dB for the through and drop ports, respectively.

B. Treated waveguide crossing

The filters of Sec. V A base their performance on the cross talk level of the waveguide crossing. If for some reason the level of cross talk is somewhat different in an actually implemented filter, e.g., because the 90-degree corners of the polymer ridge are not well defined, then the designs will not provide their nominal extinction ratio. It is therefore expedient to examine the performance of a dual-resonator add-drop filter with a treated crossing. The cross talk in this case is so small (−37 dB according to Sec. III) that any fabrication inaccuracies will not change the fact that its contribution to the interference is negligible. This time, the drop port transmission is a result of two interfering waves: the one via the resonator and the one following the Q-route. As the wave following the Q-route suffers extra propagation losses, the interference effects are bound to be relatively weak. However, we are interested in seeing whether this variant can still provide wavelength regions with high ERs for both ports.

We focus on a filter with the following geometrical parameters: $R = 5.7$ μm, $L = 0$, $g_1 = 0.3$ μm, and $g_2 = 0.48$ μm. The transmission for both ports and states is depicted in Fig. 10(a). The corresponding extinction ratios can be found in Fig. 10(b). As can be seen, extinction ratios higher than 5 dB can be provided by a wavelength range of 5 nm, accommodating six 100-GHz-spaced WDM channels.

To summarize, dual-resonator filters with perpendicular access waveguides and an untreated crossing can provide superior performance in terms of ER compared to treated-crossing ones, due to the stronger interference effects associated with the drop port transmission. However, filters of the second category can still provide high ERs for both ports over fairly broad wavelength regions. In addition, such filters do not rely on the cross talk level of the waveguide crossing, resulting in sounder designs.

VI. SUMMARY AND CONCLUSION

Several DLSPP-based thermo-optic switching elements employing microring resonators have been theoretically investigated, in pursuit of a configuration which provides high ERs for both output ports over a broad wavelength range. All simulations have been conducted by utilizing the three-dimensional vector finite-element method. The classic add-drop filter with parallel access waveguides was found inadequate due to the poor drop port ER. As a result, alternative configurations, namely add-drop filters with perpendicular access waveguides involving one and two resonators, were subsequently studied. The single-resonator add-drop filter with perpendicular bus waveguides and an untreated waveguide crossing of Sec. IV can provide extinction ratios as high as 9 dB for both output ports simultaneously. It can therefore implement an efficient 1×2 switching element. However, it cannot act as a 2×2 switch since the symmetry is broken. This task can be performed by the dual-resonator add-drop filter with perpendicular bus waveguides of Sec. V.

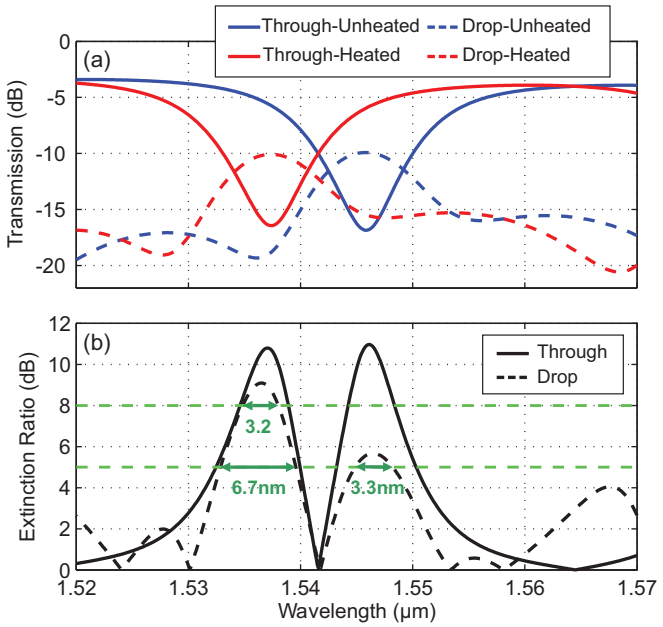

FIG. 9. (Color online) (a) Transmission vs wavelength for both output ports and both heated and unheated states. The geometrical parameters of the dual-resonator add-drop filter with perpendicular access waveguides and an untreated crossing are: $R = 5.5$ μm, $L = 0$, $g_1 = 0.3$ μm, and $g_2 = 0.5$ μm. (b) Extinction ratio vs wavelength for both ports.

Specifically, the filter of Sec. V A having an untreated waveguide crossing can provide an extinction ratio of at least 8 dB for both output ports over a wavelength range of 3.2 nm, thus readily accommodating four 100-GHz-spaced channels.

The superior performance of the filters with perpendicular access waveguides is attributed to the interference effects associated with the drop port transmission. One of the interfering waves is coming from the waveguide crossing. In order to

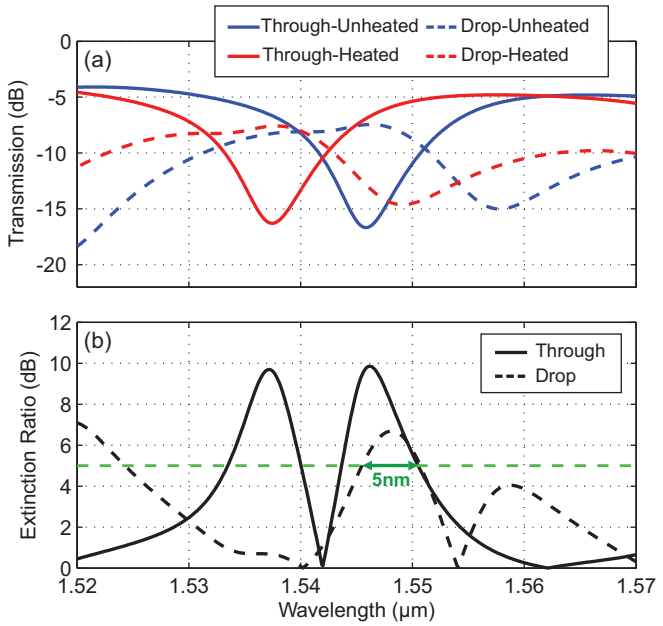

FIG. 10. (Color online) (a) Transmission vs wavelength for both output ports and both heated and unheated states. The geometrical parameters of the dual-resonator add-drop filter with perpendicular access waveguides and a treated crossing (elliptic tapering with $L_X = 6$ μm, $W_X = 1.6$ μm) are: $R = 5.7$ μm, $L = 0$, $g_1 = 0.3$ μm, and $g_2 = 0.48$ μm. (b) Extinction ratio vs wavelength for both ports.

Downloaded 18 Apr 2011 to 155.207.26.21. Redistribution subject to AIP license or copyright; see http://jap.aip.org/about/rights_and_permissions

quantify its contribution, the performance of a DLSPP waveguide crossing has been also assessed. An elliptic tapering scheme has been proposed for minimizing cross talk. Specifically, the cross talk of the treated crossing has been reduced to −37 dB, compared to −15 dB of the untreated case.

All structures considered reside on a typical silicon-on-insulator substrate. The SOI substrate is chosen in view of a prospective hybridization of the two prominent technologies for nanophotonic circuits: plasmonics and silicon photonics.[15] Moreover, this substrate provides switching times of a few microseconds, rendering the thermo-optic components capable of handling real-world routing scenarios.

ACKNOWLEDGMENTS

This work was supported in part by the European FP7 project PLATON (Contract No. 249135) and the HERACLITUS II research fellowship of the Aristotle University of Thessaloniki. The authors acknowledge Dr. N. Pleros and Professor A. Dereux for helpful discussions.

[1]S. A. Maier and H. A. Atwater, J. Appl. Phys. **98**, 011101 (2005).
[2]T. W. Ebbesen, C. Genet, and S. I. Bozhevolnyi, Phys. Today. **61**, 44 (2008).
[3]D. K. Gramotnev and S. I. Bozhevolnyi, Nat. Photonics. **4**, 83 (2010).
[4]T. Holmgaard and S. I. Bozhevolnyi, Phys. Rev. B **75**, 245405 (2007).
[5]P. Berini, Phys. Rev. B **61**, 10484 (2000).
[6]P. Berini, R. Charbonneau, N. Lahoud, and G. Mattiusi, J. Appl. Phys. **98**, 043109 (2005).
[7]T. Nikolajsen, K. Leosson, and S. I. Bozhevolnyi, Appl. Phys. Lett. **85**, 5833 (2004).
[8]G. Gagnon, N. Lahoud, G. A. Mattiussi, and P. Berini, J. Lightwave Technol. **24**, 4391 (2006).
[9]I. Breukelaar, R. Charbonneau, and P. Berini, J. Appl. Phys. **100**, 043104 (2006).
[10]T. Holmgaard, Z. Chen, S. I. Bozhevolnyi, L. Markey, A. Dereux, A. V. Krasavin, and A. V. Zayats, Appl. Phys. Lett. **94**, 051111 (2009).
[11]T. Holmgaard, Z. Chen, S. I. Bozhevolnyi, L. Markey, and A. Dereux, Opt. Express. **17**, 2968 (2009).
[12]O. Tsilipakos and E. E. Kriezis, Opt. Commun. **283**, 3095 (2010).
[13]O. Tsilipakos, T. V. Yioultsis, and E. E. Kriezis, J. Appl. Phys. **106**, 093109 (2009).
[14]J. Gosciniak, S. I. Bozhevolnyi, T. B. Andersen, V. S. Volkov, J. Kjelstrup-Hansen, L. Markey, and A. Dereux, Opt. Express. **18**, 1207 (2010).
[15]R. M. Briggs, J. Grandidier, S. P. Burgos, E. Feigenbaum, and H. A. Atwater, Nano Lett. **10**, 4851 (2010).
[16]I. I. Smolyaninov, Y.-J. Hung, and C. C. Davis, Appl. Phys. Lett. **87**, 241106 (2005).
[17]D. G. Zhang, X.-C. Yuan, A. Bouhelier, P. Wang, and H. Ming, Opt. Lett. **35**, 408 (2010).
[18]E. D. Palik, ed., *Handbook of Optical Constants of Solids*, 1st ed. (Academic Press, New York, 1985).
[19]J. Grandidier, G. Colas des Francs, L. Markey, A. Bouhelier, S. Massenot, J.-C. Weeber, and A. Dereux, Appl. Phys. Lett. **96**, 063105 (2010).
[20]O. Tsilipakos, A. Pitilakis, A. C. Tasolamprou, T. V. Yioultsis, and E. E. Kriezis, "Computational techniques for the analysis and design of dielectric-loaded plasmonic circuitry," Opt. Quant. Electron. (in press).
[21]M. A. Popović, C. Manolatou, and M. R. Watts, Opt. Express. **14**, 1208 (2006).
[22]A. V. Krasavin and A. V. Zayats, Phys. Rev. B **78**, 045425 (2008).
[23]W. Bogerts, D. Pieter, D. Van Thourhout, and R. Baets, Opt. Lett. **32**, 2801 (2007).
[24]E. Feigenbaum and M. Orenstein, Opt. Express. **15**, 17948 (2007).
[25]B. E. Little, S. T. Chu, W. Pan, and Y. Kokubun, IEEE Photon. Technol. Lett. **12**, 323 (2000).
[26]N. Sherwood-Droz, H. Wang, L. Chen, B. G. Lee, A. Biberman, K. Bergman, and M. Lipson, Opt. Express. **16**, 15915 (2008).
[27]F. Xu and A. W. Poon, Opt. Express. **16**, 8649 (2008).
[28]S. Zheng, H. Chen, and A. W. Poon, IEEE J. Sel. Top. Quantum. Electron. **12**, 1380 (2006).

Downloaded 18 Apr 2011 to 155.207.26.21. Redistribution subject to AIP license or copyright; see http://jap.aip.org/about/rights_and_permissions